The cleft ion fountain

Article

Published Version

JOURNAL OF GEOPHYSICAL RESEARCH, VOL. 90, NO. A10, PAGES 9736–9748, OCTOBER 1, 1985

The Cleft Ion Fountain

M. LOCKWOOD[1]

Space Science Laboratory, NASA Marshall Space Flight Center, Huntsville, Alabama

M. O. CHANDLER AND J. L. HORWITZ

Department of Physics, University of Alabama, Huntsville

J. H. WAITE, JR., T. E. MOORE, AND C. R. CHAPPELL

Space Science Laboratory, NASA Marshall Space Flight Center, Huntsville, Alabama

Low-energy (below approximately 50 eV) ionospheric ions, injected into the magnetosphere at the dayside cleft, are studied using data from the retarding ion mass spectrometer (RIMS) experiment on the Dynamics Explorer 1 satellite. It is concluded that upwelling ions at the cleft form an ion fountain and are blown into the polar cap by antisunward convection. At high Kp (>4), convection is generally strong enough to fill the entire polar magnetosphere with low-energy O^+ ions, whereas at low Kp (<2) they are largely restricted to the dayside half of the cap. Using a two-dimensional kinetic ion trajectory model, the locations where RIMS detected O^+ within the cap are shown to be consistent with the spatial distributions of O^+ density, predicted for an upwelling ion source at the cleft and various dawn-dusk convection electric fields. A detailed study is made of one polar pass of DE 1, during which RIMS detected He^+, N^+, O^+, and O^{++} ions, the ion trajectory model being used to trace all these ions back to a common source at an observed upwelling ion event near the cleft. All observed species are deduced to be falling earthward in the nightside of the cap, as predicted from the model, indicating the dominance of gravity over upward field-aligned acceleration (such as by the ambipolar electric field). Comparison of field-aligned velocities observed for O^+ and O^{++} ions defines a maximum limit to the upward electrostatic acceleration present within the cap which was only sufficient to eject ionospheric H^+ ions, all heavier ions being supplied from the dayside by the cleft ion fountain.

1. INTRODUCTION

The classical theory of plasma escape from the high-latitude ionsophere (the "polar wind") [*Banks and Holzer*, 1969] predicts that heavy ions are gravitationally bound and that light ions (H^+ and He^+) are expelled by the ambipolar electric field resulting from separation of electronic and ionic charges. Prior to the launch of the Dynamics Explorer satellites, no direct observations of the outflow of low-energy ionospheric ions had been made. *Hoffman and Dodson* [1980] found high-latitude light ion outflows of the magnitude predicted by Banks and Holzer; however, their analysis of the roll modulation of the ISIS 2 mass spectrometer data assumed that the ionospheric heavy ions (in particular O^+) were gravitationally bound and stationary. *Lockwood and Titheridge* [1981] and *Lockwood* [1982] deduced additional and large O^+ outflows to be present at some latitudes with high occurrence probabilities (up to 0.5) from analysis of ionospheric topside soundings. The data from the Dynamics Explorer 1 (DE 1) satellite confirmed that high-altitude polar ion flows sometimes consist almost entirely of O^+ at low energies. The energetic ion composition spectrometer (EICS) on DE 1 found that the entire spectrum could be dominated by O^+ near satellite apogee (4.5 R_E) [*Shelley et al.*, 1982] and that the occurrence probability of O^+ flows, of energies above about 10 eV, could be as large as 0.3 in the polar cap [*Yau et al.*, 1984]. The retarding ion mass spectrometer (RIMS) experiment on DE 1 found that O^+ ion flows could be dominant in the polar cap at very low energies (0–50 eV) [*Waite et al.*, 1985]. In addition, the RIMS instrument detected upward flows of O^{++} and N^+ ions [*Chappell et al.*, 1982] and of molecular ions [*Craven et al.*, 1985] in the polar magnetosphere.

Waite et al. [1985] used electric field data from the ion drift meter (IDM) on the low-altitude DE 2 satellite and concluded that for the two cases studied, the O^+ ions originated not from the entire polar cap ionsophere but from a restricted dayside source region. These ions had subsequently been swept across the cap by antisunward convection. A survey of 2 years' data from RIMS at altitudes below 2 R_E by *Lockwood et al.* [1985] identified a highly persistent source region of upflowing ionsopheric ions (of all species, including O^+) near the dayside polar cap boundary. A study of one such "upwelling ion" event by *Moore et al.* [1984] found it to be colocated with the cleft, as observed in precipitating energetic magnetosheath ions. Lockwood et al. suggested that the concept of the "geomagnetic mass spectrometer" may apply to these ionospheric ions, whereby O^+ ions are spread into the polar cap by varying amounts, depending on the strength of antisunward convection across the cap. The concept is qualitatively consistent with all features of the low-altitude RIMS data, with the energy and mass dispersions of ions seen by RIMS at great altitudes [*Moore et al.*, 1985; *Waite et al.*, 1985], and with energy dispersion seen in DE 1 high altitude plasma instrument (HAPI) observations [*Gurgiolo and Burch*, 1982]. The trajectories of such ions were modeled by *Horwitz* [1984], who predicted that the lowest-energy heavy ions could fall downward under gravity in the nightside cap, giving "parabolic" or "hopping"

[1]On sabbatical leave from Rutherford Appleton Laboratory, Chilton, Didcot, England.

Paper number 5A8486.
0148-0227/85/005A-8486$05.00

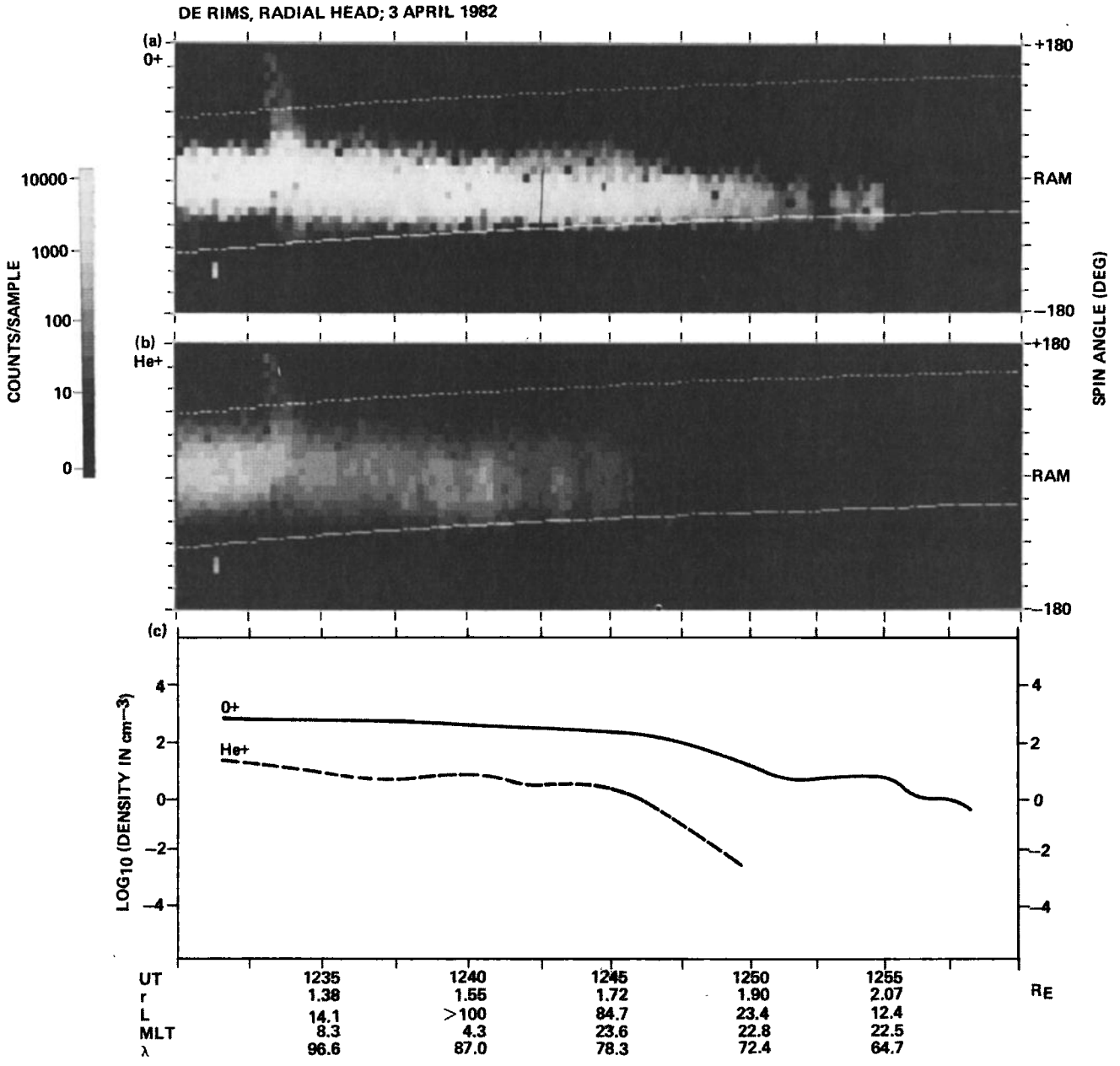

Fig. 1. Spin angle-time spectrograms for (*a*) O^+ and (*b*) He^+ ions observed by the radial head of RIMS as DE 1 traverses the southern cleft and moves into the polar cap at low altitudes; the dotted and dashed lines show the upward and downward field-aligned directions, respectively. The density of observed ions is shown in Figure 1*c* for these two species. The low-latitude edge of the upwelling ion event is encountered near 1233 UT, and O^+ is observed with densities above 1 cm^{-3} until near 1255 UT. The λ value of the satellite is defined in the text and by Figure 3.

trajectories, depending on the pitch angle of injection of the ions at the ionospheric source.

In this paper it is shown that the upwelling ion events identified in the vicinity of the cleft may be regarded as an ion fountain, supplying low-energy ions to the entire polar magnetosphere when convection is antisunward and strong. Furthermore, it is demonstrated that heavy ion flows can be downward in the polar cap, consistent with "parabolic" trajectories of heavy ions from this cleft ion fountain, as has been modeled by *Horwitz* [1984] and *Horwitz and Lockwood* [this issue].

2. Observations

The data presented here were recorded by the RIMS experiment on DE 1. A full description of the RIMS instrument is given by *Chappell et al.* [1981]. The statistical survey by *Lockwood et al.* [1985] employed observations by RIMS at low altitudes ($<2\ R_E$) between October 19, 1981, and October 19, 1983. Data were analyzed in 1-min integration periods, and in the 2 years studied, a total of 14,278 spin angle distributions were obtained at invariant latitudes greater than 40° and altitudes below $2\ R_E$. Figure 1*a* is an O^+ ion spin angle spectrogram showing a type of event which Lockwood et al. found to be present in all orbits of DE 1 which crossed the cleft in the 0600 to 1400 hours local time sector at geocentric distances, *r*, of 1.5–2.0 R_E. The event commences at 1233 UT, when the satellite crosses a sharp, distinct low-latitude boundary. Within the event the spin distribution is asymmetric and extended toward the upward field-aligned

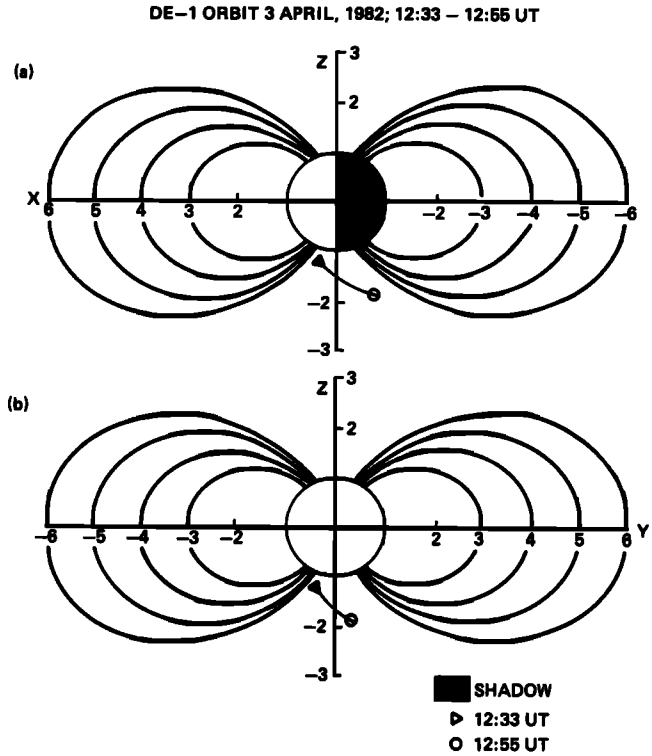

Fig. 2. DE 1 orbital segment for 1233–1255 UT, April 3, 1982, when O^+ ions were observed to the low-λ side of an upwelling ion event (see Figure 1). The orbit is projected onto the (*a*) *ZX* and (*b*) *YZ* planes of the GSM coordinate system.

direction (dashed line). By about 1235 UT the distribution is symmetric again. The asymmetry in the spin angle distribution shows that the ions are carrying upward heat fluxes [*Biddle et al.*, 1985], and the distribution functions reveal some parallel, but predominantly perpendicular, ion heating below the satellite [*Moore et al.*, 1984]; hence these events were termed "upwelling ion events" by *Lockwood et al.* [1985]. The low altitude at which the satellite encounters this upwelling ion event (geocentric distance $r = 1.33\ R_E$) is very close to the value below which their occurrence frequency falls to zero [*Lockwood et al.*, [1985]. The upwelling ion event shown in Figure 1 is relatively short-lived, partly because the spacecraft velocity is higher near perigee and partly because the events have smaller latitudinal width at lower altitudes. The spin angle spectrogram for He^+ is shown in Figure 1*b*, and the densities of these two ion species, calculated assuming that the plasma density is sufficiently high to give negative spacecraft potentials (M. O. Chandler, unpublished manuscript, 1985), are plotted in Figure 1*c*. Figure 2 shows the segment of the orbit of the DE 1 spacecraft between 1233 UT, when the lower-latitude boundary of the upwelling ion event was encountered, and 1255 UT, when the peak O^+ count rate falls below 20 counts per accumulation period (12 ms) for the last time (and the O^+ density falls below about 1 cm^{-3}): Figure 2*a* shows the projection of this orbital segment onto the *ZX* plane of the GSM coordinate system, and Figure 2*b* shows the projection onto the *YZ* plane. Figure 2*b* demonstrates that the upwelling ions are first encountered toward the dawnside of the noon-midnight meridian, but by 1255 UT the satellite was closer to that meridian and to the duskside of it. Figure 2*a* shows that O^+ ions were found up to a geocentric distance *r* of about $2\ R_E$ on the nightside of the polar cap.

The fall in the observed density of O^+ ions, detected by RIMS and shown in Figure 1*c*, may not be fully due to a decrease in the true O^+ ion density, but may be, at least in part, due to positive charging of the DE 1 spacecraft. In general, the spacecraft potential will rise with altitude to a point at which the lowest-energy ions are no longer detected by RIMS, which therefore then begins to underestimate the true ion density. This occurs when the value of the spacecraft potential (in volts) exceeds that of the ions' ram energy (in eV). Hence RIMS may have not detected O^+ after 1255 UT because densities were very low or because the energies were lower than the positive spacecraft potential or for both reasons.

3. Observations of O^+ in the Polar Cap Associated With Upwelling Ion Events

All the DE 1 orbits during which *Lockwood et al.* [1985] found upwelling ion events were studied in the same way as was the example presented in the preceding section. Hence the occurrence of polar cap O^+ flows, contiguous with upwelling ion events, was studied for the period October 1981 to October 1983. Figure 3 shows orbital segments (in both northern and southern hemispheres) of the kind shown in Figure 2*a*, i.e., in the *XZ* plane of the GSM coordinate system. The ends of these elements are defined from the RIMS observations of O^+ ions, in the same way as for Figure 2*a*. The upwelling ion events identified in the study by *Lockwood et al.* [1985] have been used, and Figure 3 shows only orbits for which RIMS monitored O^+ ions at all λ between the upwelling ion event and the equatorial plane on the nightside (λ = 0, where λ is defined by $\lambda = \tan^{-1} |Z|/X$ (see Figure 3); hence λ is zero at the nightside geomagnetic equatorial plane, 90° over either geomagnetic pole and of the order of 100° in the dayside cleft regions). A total of 68 such passes were available from the 2 years' data studied by *Lockwood et al.* [1985]. These have been sorted according to the *Kp* index value at the start time of each orbital segment. The *Kp* dependence of the spatial extent of the polar cap O^+ ions can be seen by comparing the different panels in Figure 3: O^+ is observed by RIMS at considerably smaller λ when *Kp* is high than when it is low. When *Kp* is low (<2+), observations of O^+ ions in the polar cap are restricted to a region close to the upwelling ion event, and in about half of the low-*Kp* cases they do not even extend into the nightside. At higher *Kp* (>4), however, O^+ ions are found throughout the cap, consistent with the occurrence frequency variation found by *Waite et al.* [1985]. It is not known, in general, whether or not all the cap O^+ ions originate from the upwelling ion event; however, three pieces of evidence indicate that this is usually the case. First, for the one case described in the preceding section, it is shown in section 5.2 of this paper that all ions within the cap (of all species) have velocities roughly consistent with a source at the upwelling ion event. Second, *Lockwood et al.* [1985] found very low probabilities of observing O^+ outflow at low altitudes in the polar cap, and lastly, *Waite et al.* [1985] found that for both cases they studied in detail, O^+ ions on the nightside have a dayside source near the cleft, the region of peak occurrence frequency of upwelling ion events [*Lockwood et al.*, 1985].

The locations where RIMS observed O^+ ions within the

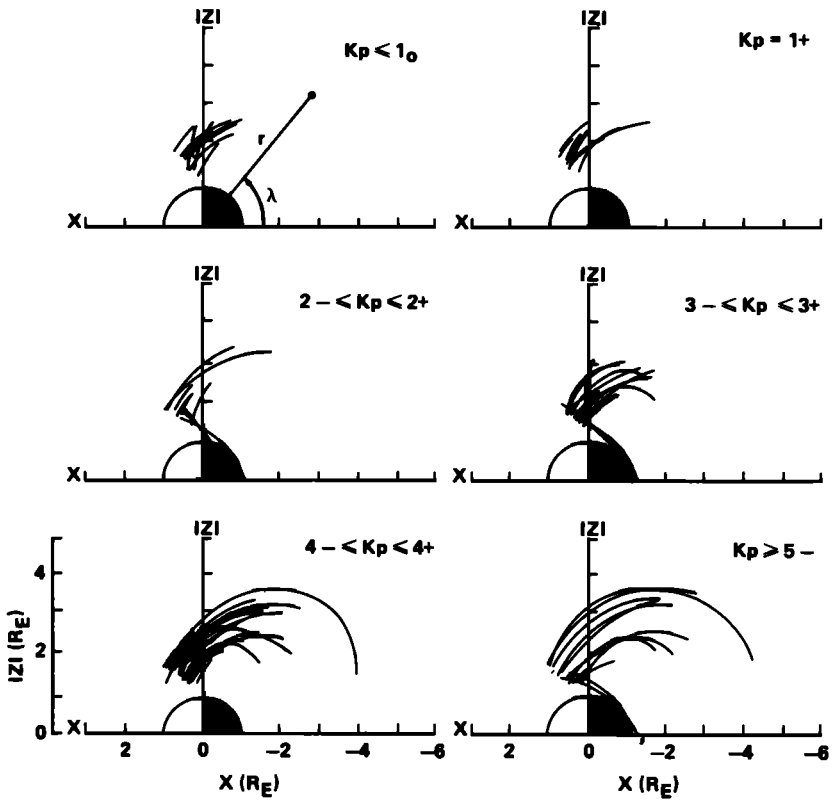

Fig. 3. DE 1 orbital segments for which O^+ ions were observed to the low-λ side of upwelling ion events. In all cases, RIMS was monitoring O^+ at all λ between the upwelling ion event and zero.

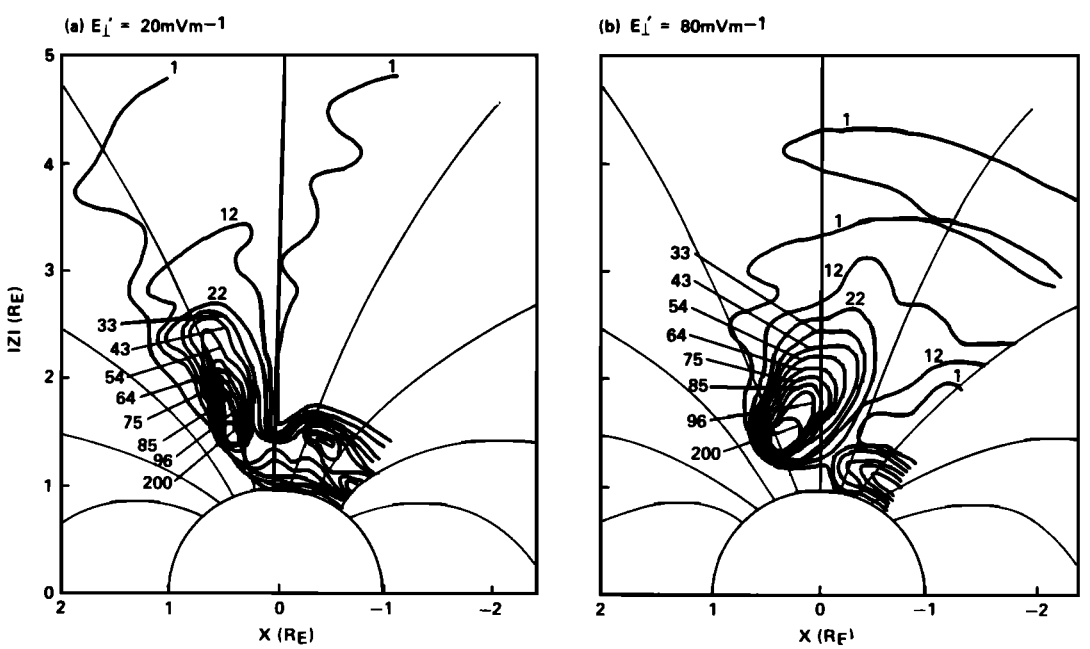

Fig. 4. Model O^+ density contours for a parallel electric field at $r = 1.05$, $E\|'$, of 0.5 μV m^{-1} and a dawn-dusk convection electric field at $r = 1.05$, $\lambda = 90°$, $E\perp'$, of (*a*) 20 mV m^{-1} (weak convection) and (*b*) 80 mV m^{-1}. The upwelling ion event is between $\lambda = 100°$ and 110° at $r = 1.4$ R_E where the O^+ density and parallel and transverse temperatures are 10^3 cm^{-3}, 1 eV, and 10 eV, respectively.

polar cap (Figure 3) are consistent with the predictions of a simulation model [*Horwitz and Lockwood*, this issue] based on the *Horwitz* [1984] ion trajectory model. In this model the location and width of an upwelling ion event are specified, along with the energy and pitch angle distributions of O^+ ions within the event. A very large number of O^+ ion trajectories are then computed for a specified value of the dawn-to-dusk convection electric field (specified at $r = 1.06$, $\lambda = 90^\circ$ and scaled elsewhere as $B^{1/2}$), using the *Horwitz* [1984] procedure. Additional allowance has been made for an electric field parallel to the magnetic field (for example, an ambipolar field), the magnitude of which is assumed to vary as r^{-2}. The density, field-aligned flux, and parallel energy of O^+ ions are then computed at points on a spatial grid and fitted with contour levels, assuming a steady state upwelling ion event source (see *Horwitz and Lockwood* [this issue] for a complete description). Figure 4 shows two sets of O^+ density contours computed for a parallel electric field at $r = 1.05$, $E\parallel'$, of 0.5 μV m^{-1} and with a perpendicular electric field (specified at $r = 1.05$, $\lambda = 90^\circ$), $E\perp'$, of 20 mV m^{-1} (Figure 4*a*) and 80 mV m^{-1} (Figure 4*b*); the two $E\perp'$ values were chosen to simulate weak and strong convection conditions, respectively. The ion source location and characteristics used were chosen to be consistent with the results of a case study of an upwelling ion event by *Moore et al.* [1984]: the source is at $r = 1.4\ R_E$ between $\lambda = 100^\circ$ and $\lambda = 110^\circ$; the O^+ ion distribution in this source region is the upward going half of a bi-Maxwellian with a parallel temperature of 1 eV and a perpendicular temperature of 10 eV; the O^+ ion density is 10^3 cm^{-3}.

Comparison of Figures 4*a* and 4*b* shows that O^+ densities greater than about 1 cm^{-3} are spread into the nightside polar cap in the high-convection case, whereas in the low-convection case they are restricted to the dayside. Note that in both cases high densities are observed at low altitudes on the nightside where ions (which had near-90° pitch angles at source) mirror, forming "hopping trajectories" [*Horwitz*, 1984; *Horwitz and Lockwood*, this issue]. The unheated F region O^+ plasma has not been included in the model and would alter the density contours at the lowest altitudes. Given that the dawn-dusk electric field increases with higher *Kp* levels [e.g., *Oliver et al.*, 1983], Figure 4 can qualitatively explain O^+ observation locations given in Figure 3. Figure 1 indicates that the sensitivity of the RIMS instrument is such that O^+ ions are observed at high altitudes over the polar cap when their density exceeds a value of the order of 1 cm^{-3}. Figure 4 shows that for weak convection, densities are only greater than 1 cm^{-3} on the dayside ($\lambda > 90^\circ$), whereas for stronger convection, such densities should be spread into the nightside cap at greater altitudes. However, there is a region near 2 R_E on the nightside where the modeled densities remain below 1 cm^{-3} in both cases, and indeed, Figure 3 reveals such a region where O^+ was never detected, despite the fact that it was traversed by all of the 68 orbits studied. The decrease in O^+ ion density shown in Figure 1*c* is of the same order of magnitude as that predicted from Figure 4; however, the initial decrease is not as rapid. Such differences could arise from the choices of O^+ source distribution function, temperatures, or electric fields $E\perp'$ and $E\parallel'$ or from the coarseness of the spatial or velocity-space grids used in the modeling.

Figure 5 is an invariant latitude–local time plot of the locations of the nightside terminators of the orbital elements shown in Figure 3 (the lowest λ at which RIMS observed O^+ ions); the solid points are for low *Kp* (<2+) and the open points for all higher *Kp* (>3-). The shaded region is where *Lockwood et al.* [1985] found the frequency of occurrence of upwelling ion events to be greater than zero. The low-λ terminators are nearly all in the premidnight sector, which is a direct consequence of the orientation of the satellite orbit and the fact that the upwelling ion events (the other ends of the orbit elements in Figure 3) are nearly all found in the prenoon sector (the shaded region). For the higher-*Kp* range, O^+ is observed to fill the whole premidnight polar cap, down to about $\Lambda = 65^\circ$. The B_Y component of the interplanetary magnetic field (IMF) may help explain this plot, owing to its effect on the asymmetry of the polar convection pattern [*Reiff and Burch*, 1985; *Zanetti et al.*, 1984; *Heelis*, 1984]. For positive B_Y, convection would mainly carry upwelling O^+ ions from their source in the morning sector into the postmidnight sector, where they would not be observed as the satellite moves into the premidnight sector. Hence for the events shown in Figures 3 and 5, upwelling O^+ ions are more likely to extend further into the nightside if B_Y is negative, when both satellite and ions move from the morning into the premidnight sector.

4. Downward Heavy Ion Flows in the Polar Cap

Figure 6 shows ion trajectories for O^+ ions, mapped using the *Horwitz* [1984] model from a source at $r_s = 1.3\ R_E$, $\lambda_s = 114^\circ$ for a convection electric field $E\perp'$ of 35 mV m^{-1} (at $r = 1.05\ R_E$ over the ionospheric pole, $\lambda = 90^\circ$), and zero parallel field $E\parallel'$. Trajectories are shown for various values of the initial ion energy at the source, ξ_i; the pitch angle of the particles is 180° at the source, i.e., upward field aligned. In all cases the upward motion of the ions is slowed by the gravitational attraction of the earth, and the lower-energy ions eventually fall back toward earth after passing through a trajectory apogee. The apogees are joined by the dashed line in Figure 6. A family of such loci of the trajectory apogees is shown in Figure 7, each curve being equivalent to the dashed curve in Figure 6, but for different values of the convection electric field $E\perp'$. The dashed curves in Figure 7 show the apogees of the O^+ ion trajectories at a fixed value of the initial ion energy at the source, ξ_i. At all λ below each solid curve the O^+ ions will be moving downward under the influence of gravity. This occurs in the region of space where densities are predicted to be low (see Figure 4), and so although such flows are predicted to exist, the flux density of ions may be low and hence difficult to detect.

Figure 8 is the same as Figure 7 but was produced using the *Horwitz and Lockwood* [this issue] model with a high parallel electric field at $r = 1.05\ R_E$ of $E\parallel' = 1.0$ μV m^{-1}. The parallel field at other heights is again assumed to obey an inverse square law dependence on r. *Barakat and Schunk* [1983] have shown that the dependence of $E\parallel$ on r is a function of the electron temperature; hence the adoption of an r^{-2} law for $E\parallel(r)$ is a crude simplification, but it does give a total ion potential curve not unlike their prediction for O^+ which remains gravitationally bound (i.e., for

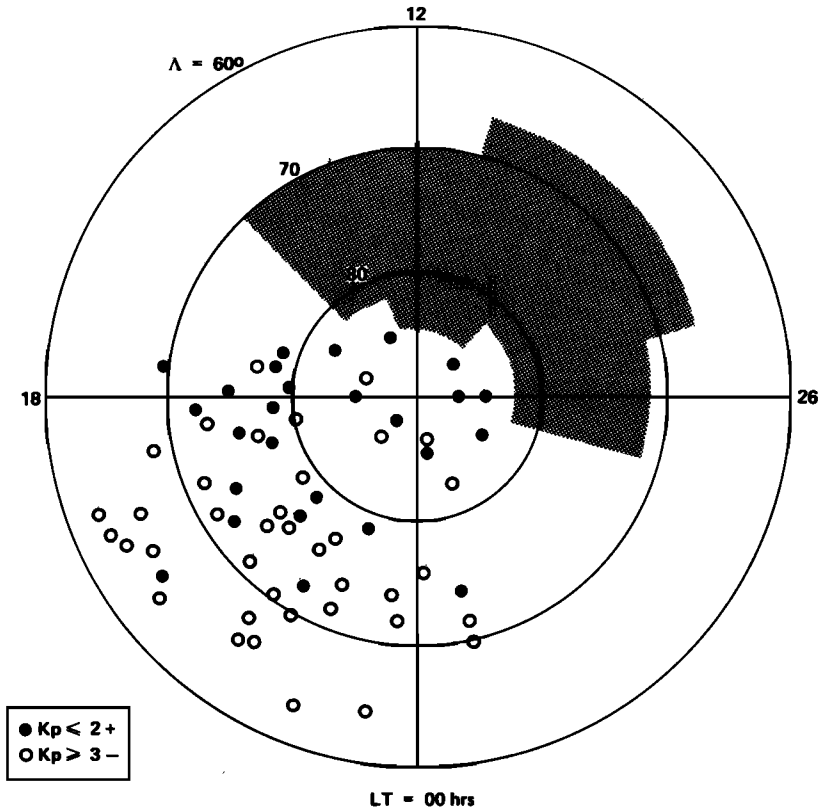

Fig. 5. Invariant latitude, local time plot of the low-λ terminations of the orbital segments shown in Figure 3, for two ranges of *Kp* value. The shaded region is where all upwelling ion events were observed by *Lockwood et al.* [1985].

moderate or low electron temperatures which are assumed to apply over the polar cap). This assumption results in a ratio of the field-aligned electrostatic force divided by the radial gravitational force f, which is independent of altitude. Figure 9 shows the linear variation of f with the value of the parallel electric field at $r = 1.05\ R_E$, $E\|'$, and is useful to explain the consequences of a certain value of $E\|'$. For example, the value of $E\|'$ of 1.0 μV m^{-1} used in Figure 8 gives f below unity for O^+ and N^+ (i.e., they are gravitationally bound) but greater than unity for H^+, He^+, and O^{++} (which are therefore expelled from the polar cap ionosphere). Figure 8 shows that this high value

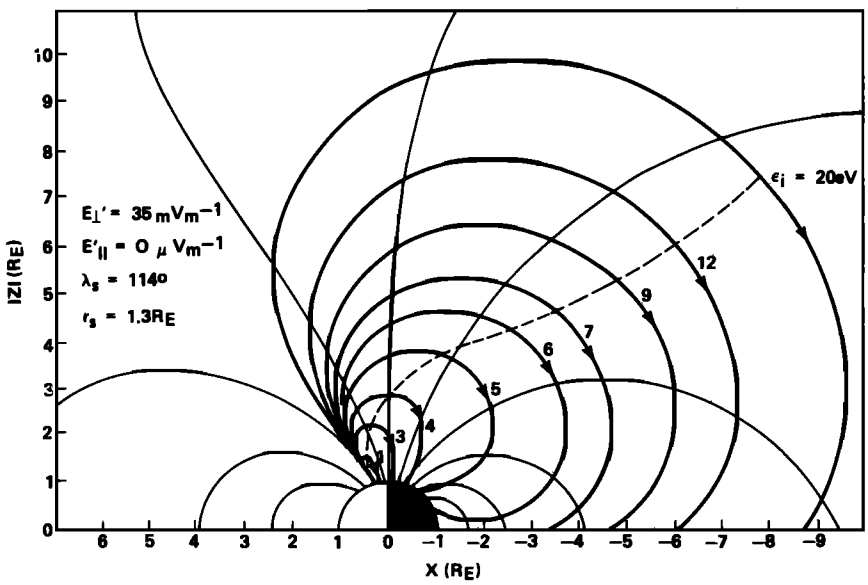

Fig. 6. O^+ ion trajectories for $E\perp' = 35$ mV m^{-1} and $E\|' = 0$ for various values of the initial ion energy at the ion source, ξ_i. The dashed curve is the focus of the trajectory apogees. Thin lines are geomagnetic field lines.

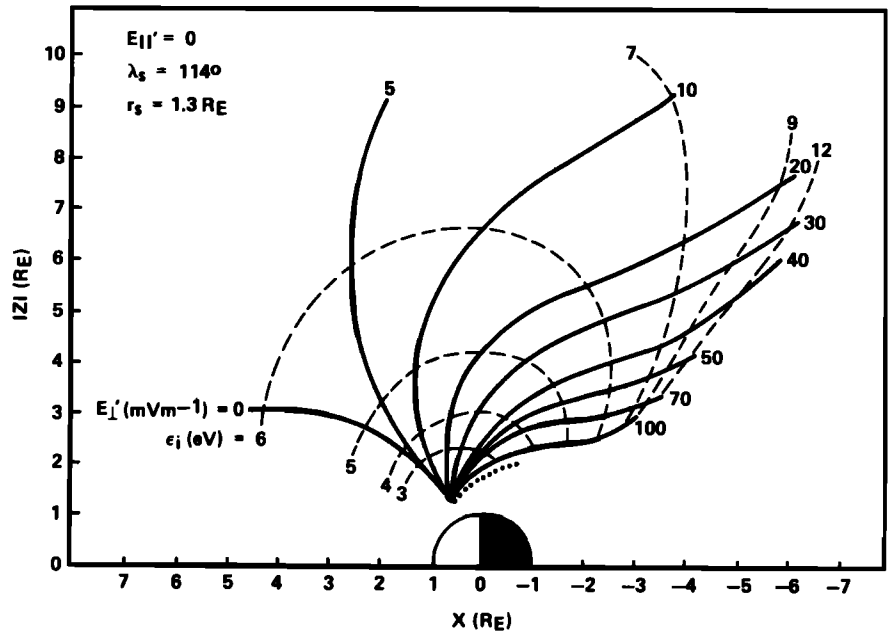

Fig. 7. Loci of trajectory apogees for various convection electric fields $E\perp'$ (solid lines) and for zero parallel electric field $E\|$. The dashed lines are the loci of apogees for various values of the initial ion energy at the souce (r_s, λ_s), ξ_i. The dotted line shows the orbital segment plotted in Figure 2*a*.

for $E\|'$ of 1 μV m^{-1} still gives regions of the cap within which O^+ ions will fall earthward. Comparison of Figures 7 and 8 shows that at higher $E\|'$ these regions of downward O^+ flow are reduced in extent, particularly for low-convection electric fields. A major difference between Figure 7 and Figure 8 is the choice of values of initial ion energies at the source, ξ_i, for which the dashed curves have been drawn; for the higher-$E\|'$ case, only the very lowest-energy ions reach apogee within the 11 R_E radial distance plotted. Hence for a given energy spectrum in the upwelling ion source region, any downward fluxes of O^+ will be reduced in magnitude for higher $E\|'$ [see *Horwitz and Lockwood*, this issue].

The orbital segment for the April 3, 1982, upwelling ion event shown in Figure 2*a* is plotted as a dotted line in Figures 7 and 8 and lies to the nightside of the solid curves for $E\perp'$ = 100 mV m^{-1} in both cases. This indicates that even a convection field of this large magnitude would be insufficient to prevent downward flow of O^+ during this event for $E\|' < 10$ μV m^{-1}. This event should, therefore, show downward flows within the cap if the electric fields do not exceed these large values. The O^+ spin angle-time

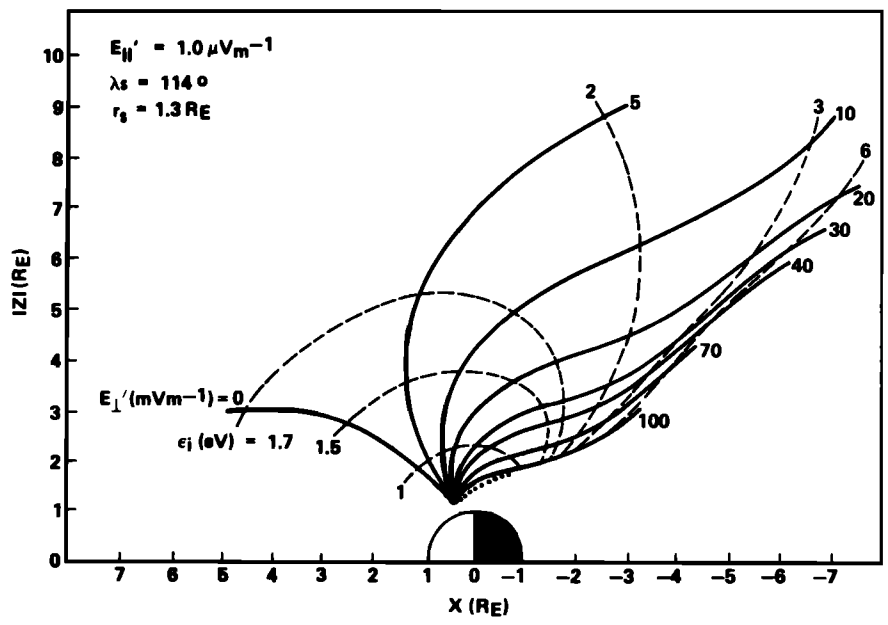

Fig. 8. Same as Figure 7, but for a parallel electric field at r = 1.05 R_E, $E\|'$, of 1.0 μV m^{-1}.

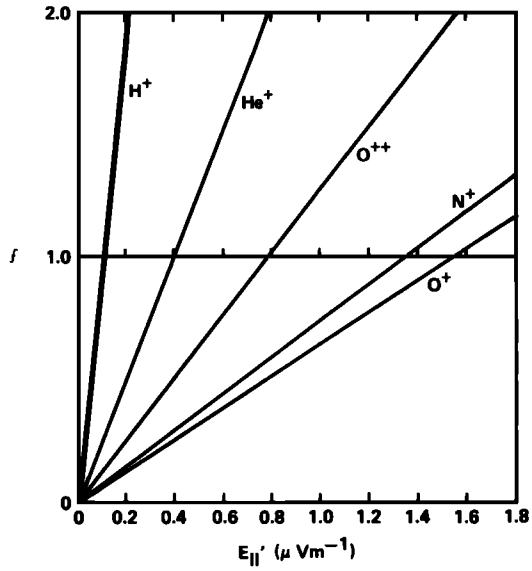

Fig. 9. The ratio of the field-aligned electrostatic force divided by the gravitational force f for an assumed r^{-2} dependence of $E\|$ and plotted as a function of the $E\|$ value at $r = 1.05\ R_E$, $E\|'$. Values are shown for the major atomic ion species observed by RIMS.

spectrogram for this event (Figure 1*a*) shows that following the upwelling ion event, the peak count rate is shifted from the ram direction toward the downward, field-aligned direction. This indicates that a downward, field-aligned flow of O^+ is present, unless there is a strong convection velocity component in the orbit plane of the satellite (M. O. Chandler, unpublished manuscript, 1985), i.e., for this orientation of the orbit, unless there is very strong anti-sunward convection. This event is studied in detail in the following section to investigate these possibilities.

5. Case Study of Heavy Ions Observed in the Southern Hemisphere Cap on April 3, 1982

The event shown in Figures 1 and 2 is a particularly good example in which to search for downward flows of heavy ions for a number of reasons. First, the satellite is near perigee, and at low altitudes the downward flow velocity should be larger. Second, the *Kp* index value was moderately high (5-), which should give convection velocities sufficiently high to disperse ions in both mass and energy yet not so high as to prevent their falling earthward under gravity before reaching the nightside auroral oval [*Horwitz and Lockwood*, this issue]. During the 5 hours prior to the RIMS observations, the ISEE 3 satellite observed the interplanetary magnetic field to have components in the GSM coordinate system, B_X, B_Y, and B_Z, which are all negative (except for the period of 1000-1145 UT, for which no data are available). This orientation of the IMF generally gives convection over the cap which is anti-sunward and toward dusk [*Heelis*, 1984], i.e., quasi-aligned with the plane of this orbit of DE 1. RIMS was operating in a "mass scan" mode, in which O^{++}, N^+, and He^+ were monitored in addition to O^+. This allows differences between ions of various mass and charge states to be

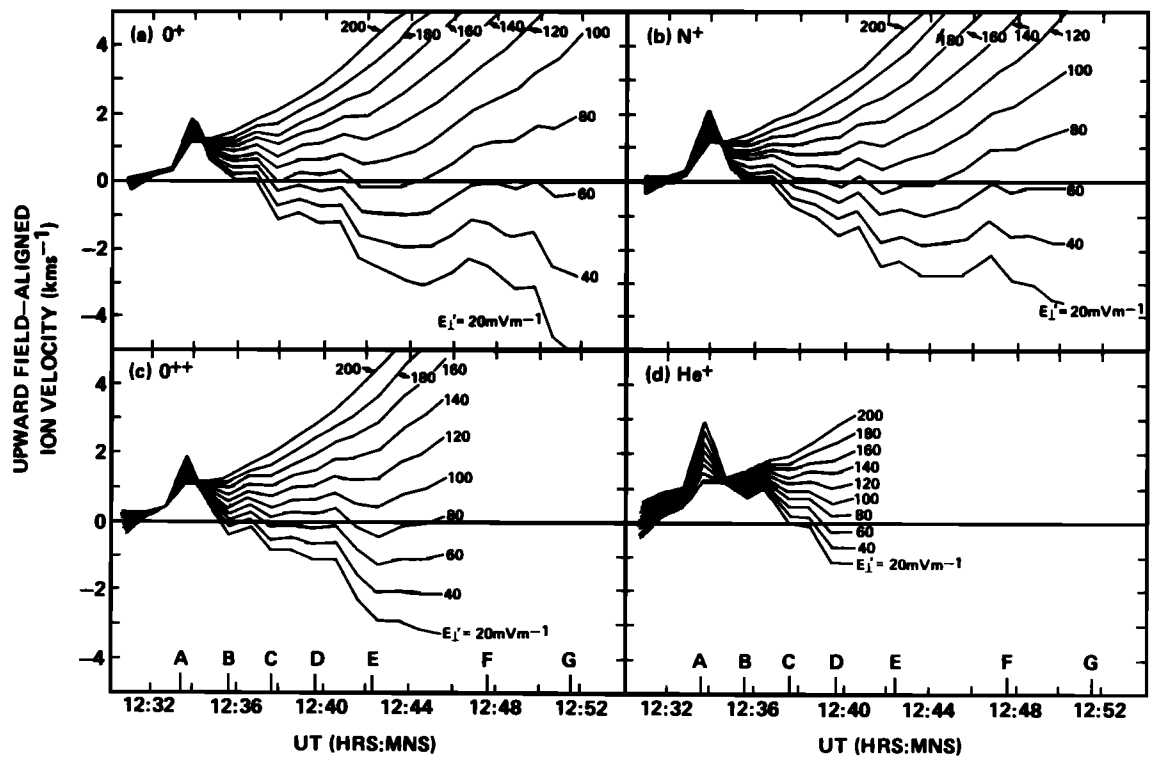

Fig. 10. The variations of field-aligned ion velocities (positive upward) during the upwelling ion event on April 3, 1982 (see Figure 1), for the observed atomic ion species (*a*) O^+, (*b*) N^+, (*c*) O^{++}, and (*d*) He^+. Values are given for various assumed values of the electric field at $r = 1.05\ R_E$, $\lambda = 90°$ perpendicular to the satellite orbit plane, $E_\perp'$, between 20 and 200 mV m^{-1}. The points A through G mark specific times in the orbit, also shown in Figure 15 and corresponding to the locations shown in Figure 11.

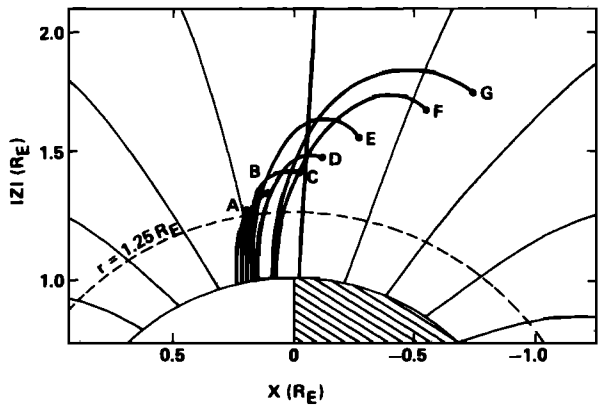

Fig. 11. O^+ ion trajectories in the GSM reference frame traced back to $r = 1.25\ R_E$ from RIMS observations at the times A through G shown in Figure 10. The ion velocities at the satellite for $E_\perp' = 60$ mV m^{-1} and the trajectories are mapped for $E_\perp' = 60$ mV m^{-1} and $E_\parallel' = 0.1$ μV m^{-1}. The thin lines are geomagnetic field lines.

exploited in the following analysis. As was discussed in the preceding section, the spin angle spectrograms give a strong indication that downward flows were indeed present.

5.1. *Ion Velocities from RIMS Observations*

Figure 10 shows the upward, field-aligned velocities for the four ion species observed during the time period of Figure 1 on April 3, 1982. The velocities are an average for the whole ion distribution and have been calculated from 1-min integrations of the RIMS data, using the method described by M.O. Chandler (unpublished manuscript, 1985). These bulk velocities have been determined for a range of $E_\perp'$, the convection electric field perpendicular to the orbit plane and normalized to the point $r = 1.05\ R_E$, $\lambda = 90°$ using a $B^{-1/2}$ dependence. The upwelling ion event is seen at 1233:30 UT (time A) in all four species as a peak in the upward flow velocity. Subsequently, for $E_\perp' < 180$ mV m^{-1} the upward velocity decreases, and for $E_\perp' < 80$ mV m^{-1} it becomes negative for the heavier ions, O^+, N^+, and O^{++} (in addition, the He^+ ions observed after 1239 UT are also moving downward for the smallest $E_\perp'$ values). It is striking how similar the velocity values for O^+, N^+, and O^{++} are at any time and $E_\perp'$; however, values for He^+ are always considerably larger. For $E_\perp'$ below about 50 mV m^{-1} the downward velocity increases almost continuously as the satellite moves poleward of the upwelling ion event. Note that the heavy ion flows are downward in the cap provided that $E_\perp'$ does not exceed 80 mV m^{-1}.

5.2. *Model Ion Trajectories and Source Locations*

The ion trajectory model of *Horwitz and Lockwood* [this issue] has been used to investigate the source of the ions detected after the upwelling ion event. This section describes how the electric fields $E_\perp'$ and $E\parallel'$ were iterated, using the ion velocity observations described in section 5.1 as inputs to the model, to give all source locations consistent with the observed upwelling ion event.

The points A–G in Figure 11 show the satellite locations, projected onto the ZX plane at the times marked in Figure 10. From each location the O^+ ion trajectory has been traced back to the ionosphere using, in this example, electric field components $E_\perp'$ and $E\parallel'$ of 60 mV m^{-1} and zero, respectively. The ion velocities at the satellite used to trace the trajectories are taken from Figure 10*a*, for the $E_\perp' = 60$ mV m^{-1} case ($E_\perp'$ is assumed not to vary during the satellite pass). Note the upward flow at A followed by downward flow at E but near-zero field-aligned flows at F and G. Figure 11 demonstrates how an ion fountain arising from the dayside source region can give such a complex velocity variation along the orbit within the cap, because of the increase in altitude of the satellite and the change in the geomagnetic dip angle.

Although all of the O^+ ions map down to the dayside and to the vicinity of the cleft, the source region has considerably greater spatial extent than is seen in the velocity measurements (Figure 10*a*). Possible causes of this anomaly are the choices for $E_\perp'$ and $E\parallel'$ or universal time or local time variations in the latitude of the source.

Use is made here of a parameter $\lambda_{1.25}$, defined as the λ value of the point where the ion trajectory crosses the $r = 1.25\ R_E$ level (i.e., an altitude of about 1600 km). This altitude has been chosen as representative of the source of upwelling ions, as *Lockwood et al.* [1985] found no upwelling ion events at lower altitudes and found that the latitudinal width of the events was smallest at this low-altitude limit. It was found that computed source locations were not sensitive to this choice for the source height.

Figure 12 shows, as a function of $E_\perp'$, the $\lambda_{1.25}$ values, calculated for O^+ observed at locations B–G shown in Figures 11 and for zero $E\parallel'$, using the Horwitz and Lockwood trajectory mapping procedure. The dashed line marked λ_{max} is the value of λ at which RIMS first observed upwelling ions; hence if $\lambda_{1.25}$ exceeds λ_{max}, the ions originated from equatorward of the upwelling ion event where no large upward flows were observed (Figure 10). For

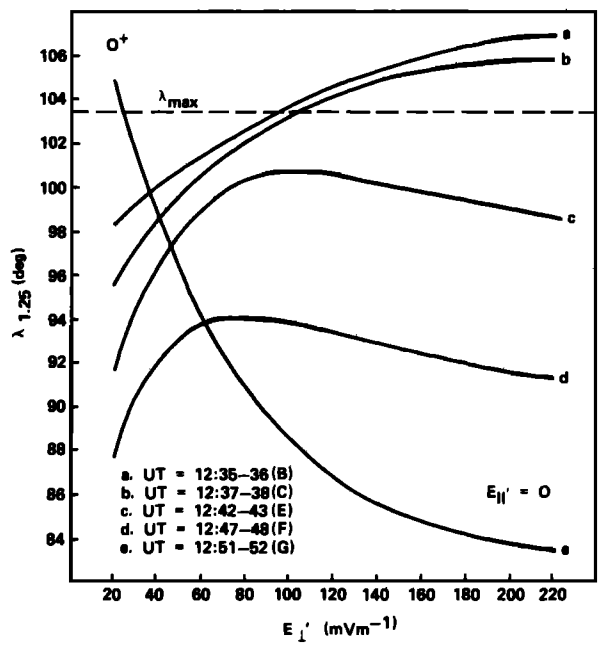

Fig. 12. The λ value of the O^+ ion trajectories at $r = 1.25\ R_E$, $\lambda_{1.25}$, as a function of the perpendicular electric field at $r = 1.05\ R_E$, $\lambda = 90°$, $E_\perp'$, for observations at five universal times shown in Figure 10 and for $E\parallel' = 0$. The λ value of the equatorward edge of the upwelling ion event is shown by λ_{max}.

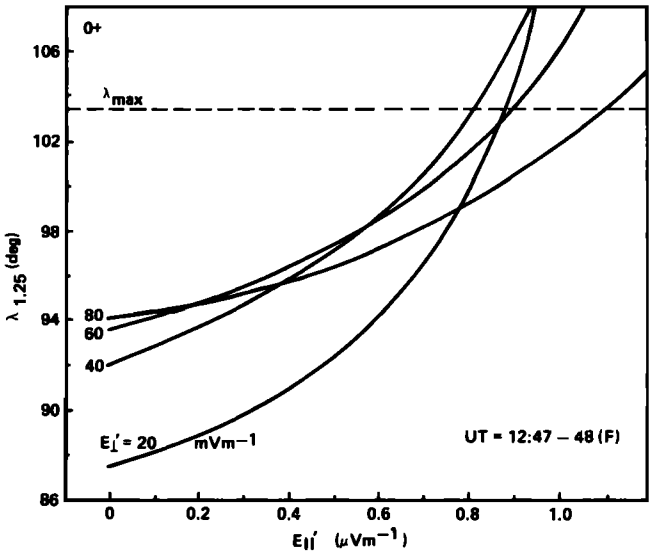

Fig. 13. The λ value of O^+ ion trajectories at $r = 1.25\ R_E$, $\lambda_{1.25}$, as a function of the parallel electric field at $r = 1.05\ R_E$, $E\parallel'$, for observations integrated over the period 1247–1248 UT (location F in Figure 11) and four values of the perpendicular field $E\perp'$.

universal times B and C the O^+ ions map to equatorward of the upwelling ion event ($\lambda_{1.25} > \lambda_{max}$) if $E\perp'$ exceeds about 100 mV m^{-1}; hence this is an upper limit to the allowed range of $E\perp'$. For these times, increasing $E\perp'$ over the shown range of realistic values causes an increase in $\lambda_{1.25}$ because the ions are convected further in rising from 1.25 R_E to the satellite. At later times (E and F), $\lambda_{1.25}$ again increases with $E\perp'$ at low values, but at the higher values it decreases again. The latter effect is due to the dependence of the ion velocity value at the satellite on $E\perp'$, which can even change sense as $E\perp'$ increases (Figure 10). At time G (the latest at which O^+ was observed) the latter effect dominates. A minimum source width is obtained for $E\perp'$ of 64 mV m^{-1} (where the source width in λ, $\Delta\lambda_{1.25}$, is 7.6°), and all ions originate from a $\lambda_{1.25}$ which is below the maximum allowed value, λ_{max}.

The curves in Figure 12 are all for zero parallel electric field. Figures 13 and 14 investigate the effect of various realistic values of $E\parallel'$ on the oxygen ion species, O^+ and O^{++}, respectively. Figure 10 shows that the velocities observed for O^+ and O^{++}, for any $E\perp'$, are very similar; this indicates that the parallel electric field must be relatively small. Figure 13 shows that the effect of increased $E\parallel'$ on the estimated O^+ source location ($\lambda_{1.25}$) is much greater at lower values of the convection field $E\perp'$. Observations at UT = 1247–1248 (point F) set a limit of about 1.0 μV m^{-1} on $E\parallel'$, for the range of $E\perp'$ allowed by Figure 12 ($E\perp' < 100$ mV m^{-1}). The effect of $E\parallel'$ on the O^{++} source location is much greater, setting a limit of between 0.2 and 0.4, depending on $E\perp'$. In both O^+ and O^{++} cases, larger $E\parallel'$ moves the source to larger λ, particularly for observations taken a large distance from the ion source. Hence using an $E\parallel'$ near these upper limits can help explain the large source width found in Figure 11 (where $E\parallel' = 0$ was used).

The effects on predicted source location, $\lambda_{1.25}$, of the electric fields, $E\perp'$ and $E\parallel'$, were studied by varying the electric fields within the range limits defined by Figures 12, 13, and 14 ($E\perp' < 100$ mV m^{-1}; $E\parallel' < 0.2$–0.4 μV m^{-1}, depending on $E\perp'$). First, $E\parallel'$ was varied at fixed values of $E\perp'$ to get minimum deviation of $\lambda_{1.25}$ for O^+ and O^{++}. The average deviation for the times A–G, shown in Figure 10, was minimized. The choice of these times weights this average to the observations nearer the upwelling ion event, when count rates are higher and velocity values therefore are more accurate. The $E\perp'$ value was similarly iterated so that O^+ and He^+ ions (i.e., ions of the same charge state but different mass) originated from the same $\lambda_{1.25}$. Figure 15 shows the results for $\lambda_{1.25}$ for the optimum pair of values, $E\perp' = 60$ mV m^{-1} and $E\parallel' = 0.1$ μV m^{-1}. The solid curve shows λ_s, the λ value of the satellite, as a function of time, and H, O, N, and the plus sign show the $\lambda_{1.25}$ values obtained by tracing He^+, O^+, N^+, and O^{++} ions, respectively, to the ionosphere using velocity estimates from 1-min integrations of the data. For any 1-min period the agreement is good, particularly nearer the upwelling ion event, between O^+, O^{++}, and He^+. Note that N^+, not used in the iterations of $E\perp'$ and $E\parallel'$, also agrees closely. At the later times the O^{++} tends to have a greater $\lambda_{1.25}$ than O^+, indicating that even the low value of 0.1 μV m^{-1} used for $E\parallel'$ may be an overestimate. Agreement is generally poorest for the last observation of a given ion species, when count rates are low and the ion velocity estimate is least reliable. In general, the different ion species map back to a source region which is in most cases of width, $\Delta\lambda_{1.25}$, less than 2° at any one time. The λ value of the computed source region decreases by about 7° in the 20 min of observation, at the end of which the ions have been mapped over about 26° of λ. The transit time of the O^+ ions at time G from $r = 1.25\ R_E$ to the satellite is 35 min (i.e., they were at $r = 1.25\ R_E$ at 1217 UT), and this is larger than the flight time of the satellite between A and G. Hence the ions observed at G left the ionosphere before those observed at A, and if the shift in the $\lambda_{1.25}$ corresponds to a real motion of the source, then it is a rapid equatorward motion in the period 1217–1233 UT.

The low-altitude (300–1300 km) DE 2 satellite was in an orbit coplanar with that of DE 1. Hence observations of the convection velocity along the DE 2 orbit give a good measurement of $E\perp'$. The best fit value for $E\perp'$ of 60 mV m^{-1} is in agreement with the observations by the IDM on DE 2 between 1223 and 1232 UT (R. A. Heelis, private communication, 1984). During this period, DE 2 traversed the invariant latitude region from 70.5° on the dayside to 76.6° on the nightside, within which DE 1 RIMS observed both the upwelling ion event and the heavy ions in the polar cap (between locations A and G in Figure 11, i.e., between 1233 and 1252 UT). The magnetic conjunction of the two satellites is not very close; however, the times of the DE 2 observations are appropriate when one remembers that the O^+ ions observed by RIMS at G were at altitudes between the two satellites between about 1217 and 1251 UT.

Note that the apparent motion of the source in the period 1217–1233 UT could equally have resulted from an increase in $E\perp'$ between 1233 and 1251 UT (which may also help explain the increased spread at later times in $\lambda_{1.25}$ values for different ion species). In addition, mapping of ion trajectories has only been performed in the noon-midnight plane, and any dawn-dusk components to the

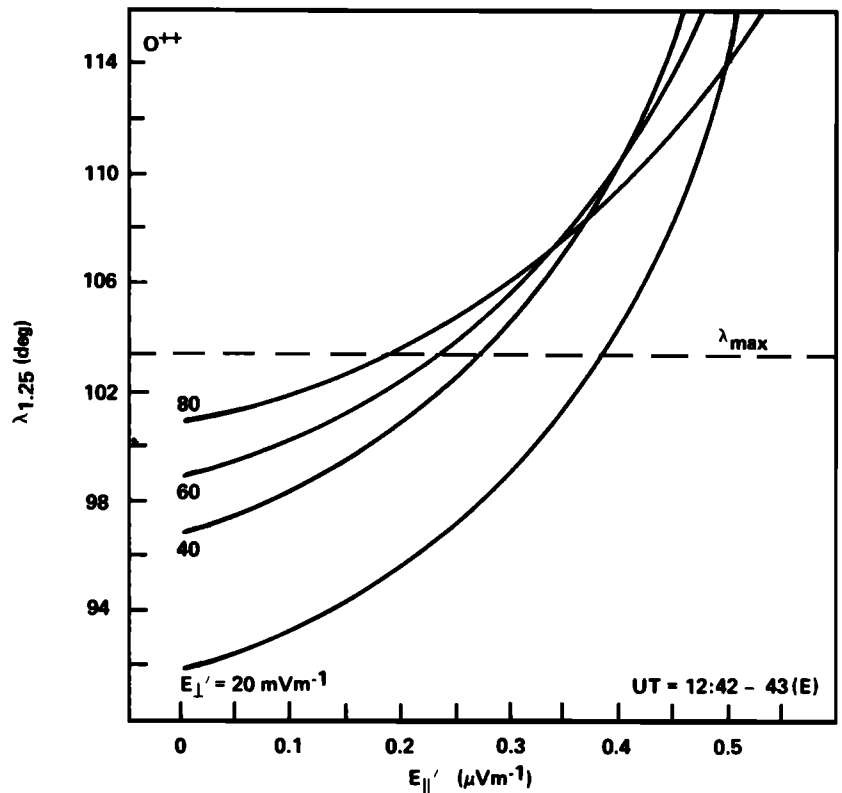

Fig. 14. Same as Figure 13, but for O^{++} ions observed over the period 1242–1243 UT (location E in Figure 11).

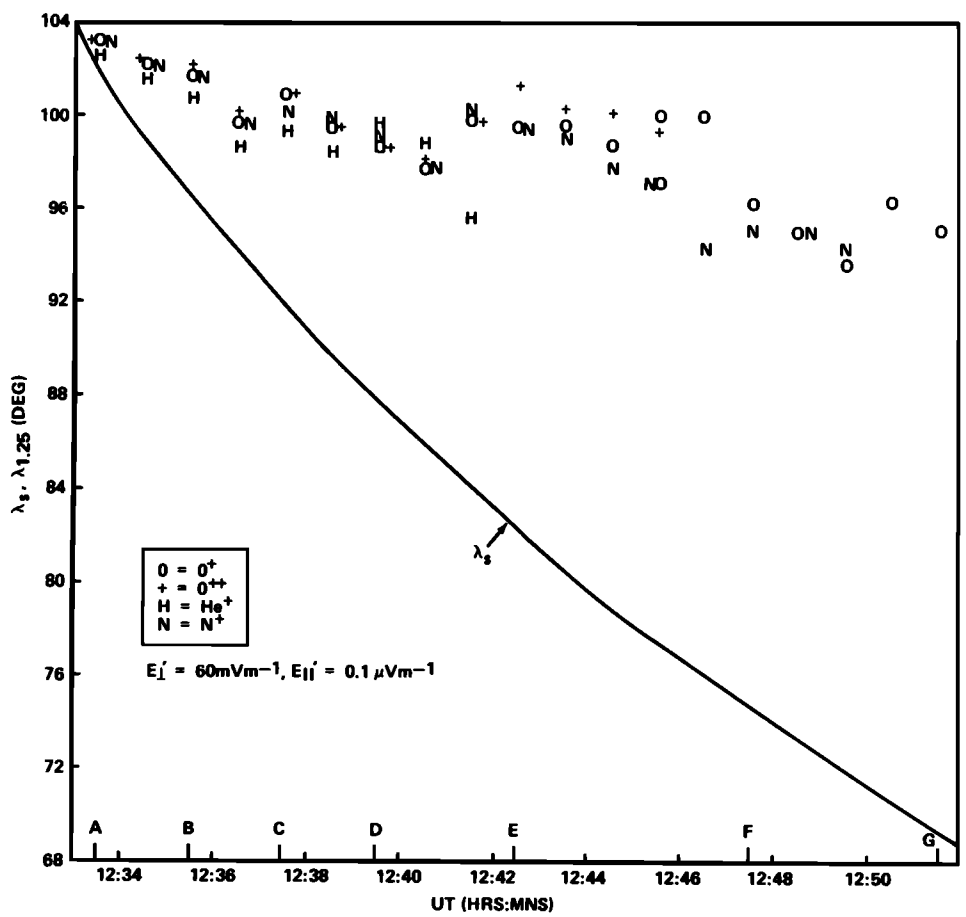

Fig. 15. The λ value of ion trajectories at $r = 1.25\ R_E$, $\lambda_{1.25}$, for 1-min integrations of data and for ion species O^+ (denoted by O), N^+ (N), O^{++} (plus sign), and He^+ (H) for best fit electric fields $E_\perp' = 60$ mV m^{-1} and $E\|' = 0.1$ μV m^{-1}. Also shown as a function of time is the λ value of the satellite location, λ_s. The times A through G refer to the times shown in Figure 10 and locations shown in Figure 11.

flow could also cause an apparent motion in $\lambda_{1.25}$: variations in $E_{\perp}'$ or in true source latitude are the only alternatives, only if the convection equipotential is aligned along the orbit plane. The DE 2 IDM observations show this not to be the case.

6. Discussion and Conclusions

Lockwood et al. [1985] identified a region in the vicinity of the dayside polar cap boundary where DE 1 RIMS regularly observed upwelling ion events, in which warmed ionospheric plasma streams upward into the magnetosphere. The low energies of these ions (typically 1–20 eV) result in trajectories which are significantly modified by high-latitude plasma convection; this is particularly true for the heavier ionspheric ion species at any given ion energy [*Horwitz*, 1984; *Horwitz and Lockwood*, this issue]. The results presented in this paper show that the combination of plasma convection, gravity, and a spatially restricted source region for most species of low-energy ions gives an effect which is analogous to a "fountain in a wind," as is illustrated schematically by Figure 14 of *Lockwood et al.* [1985]. The pieces of observational evidence for such an effect, as presented in this paper, are as follows: (1) the spreading of O^+ ions throughout the polar cap magnetosphere, contiguous with upwelling O^+ ion events, at high *Kp* (when convection is generally strong and antisunward [e.g., *Oliver et al.*, 1983]); at low *Kp* (<2), such O^+ ions are largely restricted to the dayside (see section 3); and (2) ion velocities for all species observed during an orbit over the polar cap, for which all ions are traced back to a narrow dayside source region, for a convection electric field which is consistent with DE 2 IDM observations. The velocities of the heavier ions are inferred to be downward in the nightside polar cap (section 5).

Other evidence for this effect in previous studies of RIMS data includes the following: (1) mass and energy dispersions of suprathermal ions observed poleward of the cleft at altitudes near 3.5 R_E [*Moore et al.*, 1985]; (2) dayside sources for two cases of nightside polar cap O^+ ions, deduced using simultaneous electric field observations from the DE 2 IDM experiment [*Waite et al.*, 1985]; and (3) poleward shift of the peak occurrence frequency of upwelling ion events with altitude [*Lockwood et al.*, 1985].

Together, these observations show that the upwelling ion events act as a source for suprathermal H^+, He^+, N^+, O^+, and O^{++} ions in the polar cap, forming a fountain of ions which are blown further into the cap when antisunward convection is stronger.

Lockwood et al. [1985] found the upwelling ion events in the general vicinity of the dayside cleft, and the case study by *Moore et al.* [1984] showed the event to be colocated with cleft ions seen by the DE 1 EICS instrument. Hence this source of ionospheric ions has here been termed the "cleft ion fountain."

The field-parallel electric field required to fit the RIMS ion velocity measurements ($E_{\parallel}' = 0.1\ \mu V\ m^{-1}$) is low in that, as is demonstrated by Figure 9, it is sufficient to expel only H^+, and not He^+, ions. This is consistent with the downward flows of He^+ found deep within the cap (see Figure 10*d*). No direct observations of the ambipolar field are yet available for comparison, and estimates from classical, cold polar wind models are of little relevance, as the spatial distributions of ions and electrons will have been modified, to an unknown extent, by the ion fountain itself. The dominance of gravity over upward field aligned electrostatic acceleration for all ionospheric ions heavier than H^+ can explain the downward flows of all the ions observed in the nightside cap by RIMS. In this event the total potential drop, using the $1/r^2$ form of *Horwitz and Lockwood* [this issue], is about 0.6 V. This is obviously much less than the potential drops of 5–60 V obtained by *Winningham and Gurgiolo* [1982] from atmospheric photoelectron measurements. One possible interpretation is that the large potential drops observed by *Winningham and Gurgiolo* [1982] are located above the DE 1 measurements considered here. We note that detailed study of ion velocities for various ion species in the ion fountain could in the future be used to give the first experimental estimates for the ambipolar electric field in the polar magnetosphere.

Acknowledgments. The authors are grateful to the RIMS team at Marshall Space Flight Center and the programming staff of Intergraph and Boeing Corporation for assistance with the data reduction software. We would also like to thank R. A. Heelis for useful discussions and for supplying DE 2 IDM observations. Support for M. Lockwood and M. O. Chandler came from the National Research Council, under their Resident Research Associateship program, and for J. L. Horwitz, from NASA contract NAS8-33982 at the University of Alabama in Huntsville.

The Editor thanks J. Burch and N. Singh for their assistance in evaluating this paper.

References

Banks, P. M., and T. E. Holzer, High-latitude plasma transport: The polar wind, *J. Geophys. Res.*, *74*, 6317, 1969.

Barakat, A. R., and R. W. Schunk, O^+ ions in the polar wind, *J. Geophys. Res.*, *88*, 7887, 1983.

Biddle, A. P., T. E. Moore, and C. R. Chappell, Occurrences of ion heat fluxes in the light ion polar wind (abstract), *Eos Trans. AGU*, *66*, 338, 1985.

Chappell, C. R., S. A. Fields, C. R. Baugher, J. H. Hoffman, W. B. Hanson, W. W. Wright, and H. D. Hammack, The retarding ion mass spectrometer on Dynamics Explorer-A, *Space Sci. Instrum.*, *5*, 477, 1981.

Chappell, C. R., R. C. Olsen, J. L. Green, J. F. E. Johnson, and J. H. Waite, Jr., The discovery of nitrogen ions in the earth's magnetosphere. *Geophys. Res. Lett.*, *9*, 937, 1982.

Craven, P. D., R. C. Olsen, C. R. Chappell, and L. Kakani, Observations of molecular ions in the earth's magnetosphere, *J. Geophys. Res.*, in press, 1985.

Gurgiolo, C., and J. L. Burch, DE-1 observations of the polar wind – A heated and unheated component, *Geophys. Res. Lett.*, *9*, 945, 1982.

Heelis, R. A., The effects of interplanetary magnetic field orientation on dayside high-latitude ionospheric convection, *J. Geophys. Res.*, *89*, 2873, 1984.

Hoffman, J. H., and W. H. Dodson, Light ion concentrations and fluxes in the polar regions during magnetically quiet times, *J. Geophys. Res.*, *85*, 626, 1980.

Horwitz, J. L., Features of ion trajectories in the polar magnetosphere, *Geophys. Res. Lett.*, *11*, 701, 1984.

Horwitz, J. L., and M. Lockwood, The cleft ion fountain: A two-dimensional kinetic model, *J. Geophys. Res.*, this issue.

Lockwood, M., Thermal ion flows in the topside auroral ionsophere and the effects of low-altitude, transverse acceleration, *Planet. Space Sci.*, *30*, 595, 1982.

Lockwood, M., and J. E. Titheridge, Ionospheric origin of magnetospheric O^+ ions, *Geophys. Res. Lett.*, *8*, 381, 1981.

Lockwood, M., J. H. Waite, Jr., T. E. Moore, J. F. E. Johnson, and C. R. Chappell, A new source of suprathermal O^+ ions near the dayside polar cap boundary, *J. Geophys. Res.*, *90*, 4099, 1985.

Moore, T. E., J. H. Waite, Jr., M. Lockwood, M. O. Chandler, C. R. Chappell, M. Sugiura, D. R. Weimer, and W. K. Peterson, Upwell-

ing O^+ ions: A case study (abstract), *Eos Trans. AGU, 65,* 1056, 1984.

Moore, T. E., C. R. Chappell, M. Lockwood, and J. H. Waite, Jr., Superthermal ion signatures of auroral acceleration processes, *J. Geophys. Res., 90,* 1611, 1985.

Oliver, W. L., J. M. Holt, R. H. Ward, and J. V. Evans, Millstone Hill incoherent scatter observations of auroral convection over $60° < \Lambda < 75°$, 3, Average patterns versus *Kp*, *J. Geophys. Res., 88,* 5505, 1983.

Reiff, P. H., and J. L. Burch, IMF B_y-dependent plasma flow and Birkeland currents in the dayside magnetosphere, 1, Dynamics Explorer observations, *J. Geophys. Res., 90,* 1595, 1985.

Shelley, E. G., W. K. Peterson, A. G. Ghielmetti, and J. Geiss, The polar ionosphere as a source of energetic magnetospheric plasma, *Geophys. Res. Lett., 9,* 941, 1982.

Waite, J. H., Jr., T. Nagai, J. F. E. Johnson, C. R. Chappell, J. L. Burch, T. L. Killeen, P. B. Hays, G. R. Carignan, W. K. Peterson, and E. G. Shelley, Escape of suprathermal O^+ ions in the polar cap, *J. Geophys. Res., 90,* 1619, 1985.

Winningham, J. D., and C. Gurgiolo, DE-2 Photoelectron measurements consistent with a large scale parallel electric field over the polar cap, *Geophys. Res. Lett., 9,* 977, 1982.

Yau, A. W., B. A. Whalen, W. K. Peterson, and E. G. Shelley, Distribution of upflowing ionospheric ions in the high-altitude polar cap and auroral ionosphere, *J. Geophys. Res., 89,* 5507, 1984.

Zanetti, L. J., T. A. Potemra, T. Iijima, W. Baumjohann, and P. F. Bythrow, Ionospheric and Birkeland current distributions for northward interplanetary magnetic field: Inferred polar convection, *J. Geophys. Res., 89,* 7453, 1984.

M. O. Chandler and J. L. Horwitz, Department of Physics, University of Alabama, Huntsville, AL 35899.

C. R. Chappell, M. Lockwood, T. E. Moore, and J. H. Waite, Jr., Space Science Laboratory, NASA Marshall Space Flight Center, Huntsville, AL 35812.

(Received January 18, 1985;
revised April 8, 1985;
accepted April 23, 1985.)